Raman electron paramagnetic resonance in $Zn_{1-x}Co_xTe$ and $Cd_{1-x}Co_xTe$

M. J. Seong, H. Alawadhi, I. Miotkowski, and A. K. Ramdas
Department of Physics, Purdue University, West Lafayette, Indiana 47907

S. Miotkowska
Institute of Physics, Polish Academy of Sciences, AL. Lotnikow 32/46, 02-668 Warsaw, Poland
(Received 27 July 2000; published 13 March 2001)

Electronic Raman transitions due to the spin flip of the $3d$ electrons of Co^{2+} in $Zn_{1-x}Co_xTe$ and $Cd_{1-x}Co_xTe$ ($x \leqslant 0.01$) are observed at $\hbar\omega_{PM} = g(Co^{2+})\mu_B H$ with $g(Co^{2+}) = 2.295 \pm 0.010$ and 2.310 ± 0.002, respectively. The intensity of Raman electron paramagnetic resonance (Raman-EPR) shows strong resonant enhancement when the incident or scattered photon energy coincides with that of a Zeeman component of the free exciton. Under resonant conditions, the Raman spectra display ''ZnTe-like'' (or ''CdTe-like'') and ''CoTe-like'' longitudinal optical (LO) phonons in combination with the spin-flip transitions, a consequence of the Fröhlich interaction. In $Zn_{1-x}Co_xTe$, even the ZnTe-like TO phonon exhibited EPR sidebands but mediated by the deformation potential; the large p-d spin-spin exchange interaction in Co^{2+}-based II-VI diluted magnetic semiconductors is the underlying microscopic mechanism.

DOI: 10.1103/PhysRevB.63.125208 PACS number(s): 78.30.Fs, 75.50.Pp, 76.30.Fc

I. INTRODUCTION

In diluted magnetic semiconductors (DMS's), where the cations in a tetrahedrally coordinated II-VI semiconductor are randomly replaced by a member of the $3d$-transition metal ions (TMI's), the two $4s$ electrons participate in the tetrahedral bonding scheme, whereas the $3d$ electrons remain localized around the TMI subject to the crystal field. The TMI's are typically characterized by a large magnetic moment. In contrast to their nonmagnetic counterparts such as $Cd_{1-x}Zn_xTe$, the II-VI DMS alloys exhibit remarkable magnetic and magneto-optic properties,[1] originating in the ''effective'' spin-spin interaction between the band electrons and the $3d$ electrons of the TMI, the so-called *sp-d exchange interaction*.[2] The most extensively studied DMS's are the II-VI ternaries with Mn^{2+}, which with its half filled $3d$ shell display a total spin of $S = 5/2$ and $L = 0$ in its ground state and a magnetic moment of $5.92\mu_B$, where μ_B is the Bohr magneton. They exhibit a huge *effective g* factor for the band electrons, often as high as two orders of magnitude larger than that for the non-magnetic host II-VI semiconductors. In contrast, the g factor of the $3d$ electrons of Mn^{2+}, for example, is approximately two. The ground state of Mn^{2+} splits into its Zeeman sublevels under the external magnetic field and the inelastic light scattering from the magnetic excitations involving these Zeeman sublevels is known as Raman electron paramagnetic resonance (Raman-EPR).[3] The Raman-EPR is a powerful spectroscopic technique in the study of the magnetic splittings of the ground state of a TMI in II-VI DMS's, its excitonic resonance enhancement, and its interaction with phonons.[4]

The other TMI's have been much less studied, mainly due to their lower solubility limit in the II-VI's and the technological difficulties in growing crystals based on them.[5] Given this background, the recent success in the growth of $Zn_{1-x}Co_xTe$ and $Cd_{1-x}Co_xTe$ with significantly high Co^{2+} concentration in our crystal growth facility[6] provided a unique scientific opportunity to explore and delineate the magnetic excitations in the Co-based *zinc-blende* DMS's. Such an investigation, besides expanding the scope of the subject, has a special appeal in view of the electronic energy level structure of Co^{2+} in contrast to that of Mn^{2+}. More specifically, the focus of this paper is the Raman-EPR of the $3d$ electrons of Co^{2+} in $Zn_{1-x}Co_xTe$ and $Cd_{1-x}Co_xTe$ and its striking resonant enhancement when the energy of the scattered photon equals that of a Zeeman component of the free exciton, which is measured with wavelength modulated reflectivity.

II. EXPERIMENT

Single crystals of $Zn_{1-x}Co_xTe$ and $Cd_{1-x}Co_xTe$ were grown using the Bridgman technique. The wavelength modulated reflectivity spectra were recorded using a SPEX (Model 1870) 0.5 m monochromator with a tungsten lamp. A vibrating mirror inside the monochromator modulated the wavelength of the monochromatized light at 85 Hz. The light reflected by the optical specimen was detected with a silicon photodiode followed by a lock-in amplifier. The sample was typically cooled down to a temperature (T) of 10 K in a Janis Superconducting Magnet cryostat. A SPEX (Model 14018) 0.85 m double-grating monochromator and an RCA (type C31034A) photomultiplier with a standard photon counting electronics were used for photoluminescence and Raman measurements. The samples were excited with 514.5 and 501.7 nm lines from a Spectra-Physics Ar^+ laser or continuously tuned monochromatic light from a Coherent CR899 tunable Ti:sapphire laser.

III. RESULTS AND DISCUSSION

A. Electronic level structure of Co^{2+} with T_d site symmetry

The energy level spectra and the associated magnetic properties of substitutional Co^{2+} in DMS's with T_d site symmetry have been studied by Villeret *et al.*[7] The electronic configuration of Co^{2+} is $[Ar]3d^7$ with $^4F_{9/2}$ ground state. The total orbital angular momentum $L = 3$ and total spin angular momentum $S = 3/2$ give a 28-fold degeneracy to the

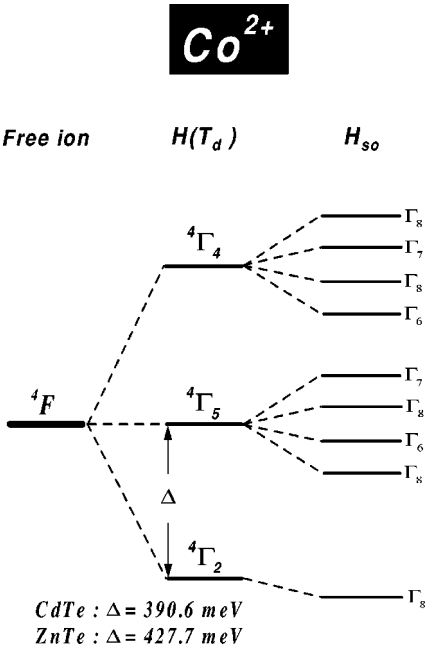

FIG. 1. Schematic diagram of the energy levels of Co^{2+} in the zinc-blende $Zn_{1-x}Co_xTe$ and $Cd_{1-x}Co_xTe$ taking into account crystal field and the spin-orbit splitting. (After Ref. 7.)

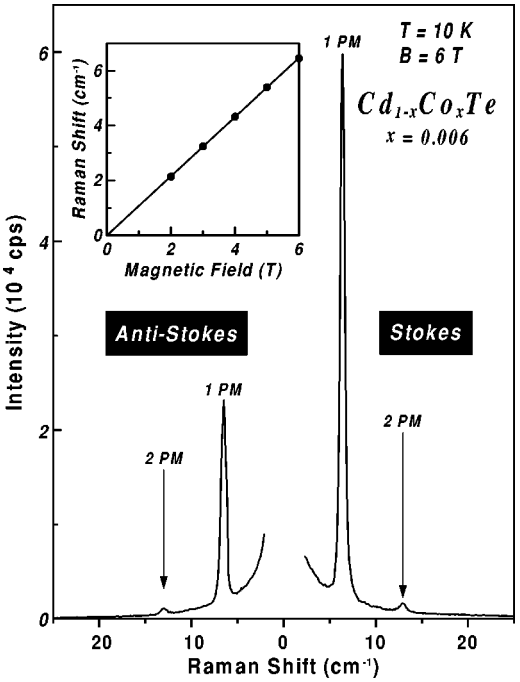

FIG. 2. Stokes (S) and anti-Stokes (AS) Raman lines at ω_{PM} generated by spin-flip transitions within the Zeeman multiplet of Co^{2+} in $Cd_{1-x}Co_xTe$ with $x=0.006$. The energy of the exciting laser line $\hbar\omega_L=1.605$ eV; the applied magnetic field $H=6$ T.

$^4F_{9/2}$ ground state. Under the influence of the crystal field of the T_d site symmetry that characterizes Co^{2+} in CdTe and ZnTe, the sevenfold orbital degeneracy splits into a $^4\Gamma_2$ singlet, a $^4\Gamma_5$ triplet, and a $^4\Gamma_4$ triplet in the order of increasing energy. The energy separation between the first two crystal field split levels, the ground state $^4\Gamma_2$ and the first excited state $^4\Gamma_5$, Δ, is 390.6 and 427.7 meV for CdTe and ZnTe, respectively.[8] Therefore, only the ground state is populated at low temperatures. Spin-orbit coupling then splits both $^4\Gamma_5$ and $^4\Gamma_4$ into $\Gamma_6+\Gamma_7+2\Gamma_8$ levels as shown in Fig. 1. The ground state $^4\Gamma_2$ does not split but becomes Γ_8, retaining its fourfold spin degeneracy, leading to the low-temperature paramagnetism of Co^{2+} ion with an effective spin $S=3/2$.

B. Raman-EPR of Co^{2+} in CdTe and ZnTe

In dilute concentrations, the Co^{2+} ions are sufficiently apart, causing the exchange interaction between them to be negligible; the ions can thus be treated as being independent. The application of an external magnetic field **H** removes the fourfold degeneracy of the Γ_8 ground state at E_0, the energies of the Zeeman sublevels being given by $E(m_S)=E_0+g\mu_B H m_S$, where g is the Landé g factor of the Co^{2+} ion and m_S the projection of **S** along **H** is $-3/2$, $-1/2$, $+1/2$, or $+3/2$. The electron spin-flip transitions between adjacent sublevels of this Zeeman multiplet can then be observed as Raman-EPR shifts; the results for $Cd_{1-x}Co_xTe$ are shown in Fig. 2. Both Stokes and anti-Stokes components are observed with a Raman shift of $\omega_{PM}=(6.40\pm0.04)$ cm^{-1} at 10 K with $H=6$ T for $\Delta m_S=\pm1$, respectively; here, PM stands for paramagnetic. The polarization dependence of the Stokes and the anti-Stokes Raman-EPR lines in $Cd_{1-x}Co_xTe$, with the scattering geometry shown in Fig. 3, is displayed in Fig. 4. The small Co^{2+} concentration (x) compelled us to employ an excitonic resonance condition to observe the Raman-EPR lines. However, the short penetration depth of, and the small volume probed by, the incident laser radiation led to a departures from the exact $(\hat{\sigma}_{\pm},\hat{z})$ configuration. The Stokes line is observed strongly but with a small leakage of the anti-Stokes component in $(\hat{\sigma}_{+},\hat{z})$, whereas in $(\hat{\sigma}_{-},\hat{z})$ the anti-Stokes line is dominant and the Stokes much weaker. The ''leakage'' observed in both configurations can be attributed to departures from the exact right-angle geometry.

The Raman EPR of the $3d$ electrons of Co^{2+} in $Cd_{1-x}Co_xTe$ can be explained either by invoking a virtual transition to one of its excited states or through virtual interband transitions, together with the s-d or the p-d exchange interaction.[9] Although both mechanisms predict the experimentally observed polarization characteristics of the Stokes and anti-Stokes components of the Raman-EPR lines correctly, only the latter is consistent with the observed resonant enhancement in the intensity of the Raman-EPR lines as the laser energy ($\hbar\omega_L$) approaches the excitonic energy gap (E_{Xg}). Hence, only the latter mechanism involving interband transitions will be discussed in what follows. It involves the exchange interaction between the excited electron and Co^{2+}, which raises the spin of a Co^{2+} ion while simultaneously lowering that of the band electron or vice versa, leading to $\Delta m_S(Co^{2+})=\pm1$ and $\Delta m_J(e)=\mp1$. In Fig. 3, one of the several such virtual transitions[9] is schematically illustrated for both the Stokes and the anti-Stokes processes with the right-angle geometry shown in the box. In the presence of a magnetic field, the Γ_8 valence band splits into four subbands, and the Γ_6 conduction band splits into two subbands. In the

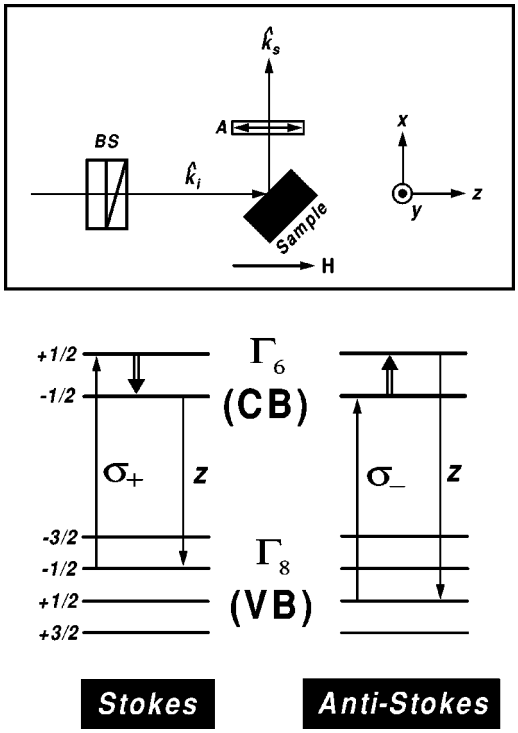

FIG. 3. Raman mechanism for the ω_{PM} line involving the band electrons. *CB* and *VB* refer to the conduction and valence bands, respectively, which are labeled by the electronic magnetic quantum number m_J. The single arrows indicate virtual electric dipole transitions, while the double arrows refer to transitions induced by the band-electron-Co^{2+} exchange interaction. In the box, the geometry for Raman scattering in the presence of a magnetic field with $(\hat{\sigma}_{\pm},\hat{z})$ polarizations for the incident and scattered light, respectively. *BS* stands for the Babinet-Soleil compensator and *A* for an analyzer. The axes are chosen such that $\hat{z}$ is parallel to **H**.

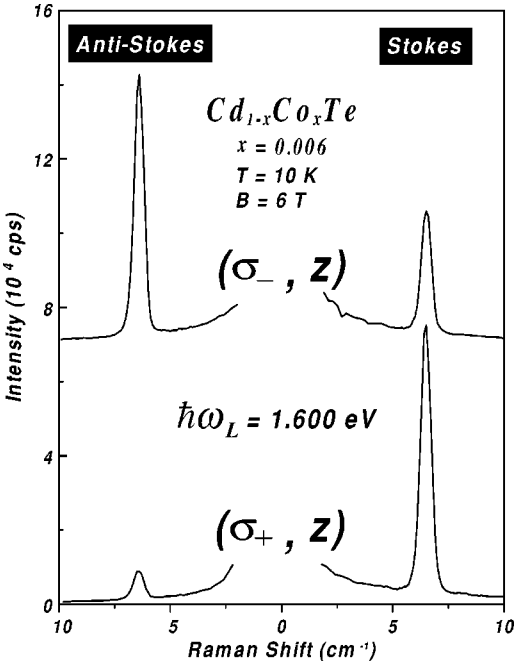

FIG. 4. Polarization dependence of the Stokes (*S*) and anti-Stokes (AS) Raman lines at ω_{PM} generated by spin-flip transitions within the Zeeman multiplet of Co^{2+} in $Cd_{1-x}Co_xTe$ with $x=0.006$. The energy of the exciting laser line $\hbar\omega_L=1.600$ eV; the applied magnetic field $H=6$ T with the scattering geometry as shown in Fig. 3. The base lines are shifted vertically for clarity.

first step of the Stokes process, an incident photon of polarization $\hat{\sigma}_+$ is absorbed, exciting an electron to the conduction band with $\Delta m_J=+1$ and creating a hole in the valence band. In the second step, the excited electron interacts with a Co^{2+} ion via spin-spin exchange coupling, resulting in $\Delta m_S(Co^{2+})=+1$ and $\Delta m_J(e)=-1$. Finally, the electron and the hole recombine emitting a photon of energy $\hbar\omega_s=\hbar\omega_i-\hbar\omega_{\mathrm{PM}}$ of polarization $\hat{z}$; the band electron has thus returned to its ground state, but leaves the Co^{2+} ion in the next sublevel of the Zeeman multiplet. Note that the electronic transitions are *virtual*, with energy being conserved only in the overall scattering process. In the same manner, the anti-Stokes process occurs as shown in Fig. 3, deexciting the Co^{2+} ion to the next lower sublevel of the Zeeman multiplet. The Raman-EPR signatures for $Zn_{1-x}Co_xTe$ are displayed in Fig. 5.

For both CdTe and ZnTe, $\hbar\omega_{\mathrm{PM}}$ is linear in H within experimental errors as shown in the insets of Figs. 2 and 5, respectively. The g factors for Co^{2+}, extracted from our Raman-EPR measurements, are 2.310 ± 0.002 in CdTe and 2.295 ± 0.010 in ZnTe, in excellent agreement with the values from microwave electron-spin resonance measurements, viz., 2.3093 and 2.2972, respectively.[10] They are significantly larger than the g factor of 2.0 for Mn^{2+} in Mn-based DMS as expected for its $^6S_{5/2}$ ground state.[9] The deviation of the g factor from the spin-only value of 2 results from the mixing of the ground state with the higher-lying orbital states by the spin-orbit interaction. For Mn^{2+} in zinc-blende semiconductors with T_d-site symmetry, the mixing of the ground state with higher-lying orbital states is negligible, due to the large value of $\Delta_{Mn^{2+}}\simeq2.4$ eV, thus yielding $g=2.0$. For Co^{2+} in the same environment ($\Delta_{Co^{2+}}\simeq0.4$ eV), the mixing cannot be ignored and accounts for the increase of the g factor by ~0.3. It is very interesting to note that multiples of $\hbar\omega_{\mathrm{PM}}$ up to the fourth order are clearly observed as Raman shifts. In order to explain Raman transitions with shifts of $n\hbar\omega_{\mathrm{PM}}$ $(n=3,4)$, which do not satisfy the angular momentum conservation unlike the $\hbar\omega_{\mathrm{PM}}$ and $2\hbar\omega_{\mathrm{PM}}$ transitions, it is necessary to invoke a new microscopic mechanism.[11,12] Peterson *et al.*[11] observed Raman-EPR signatures of Mn^{2+} with shifts of $n\hbar\omega_{\mathrm{PM}}$ $(n=3,4)$ and accounted for the multiple spin-flip features in terms of excitations within nearest-neighbor Mn^{2+} pairs coupled via *d-d* exchange interaction in $Cd_{1-x}Mn_xTe$. Therefore, the multiple Raman-EPR signatures observed in $Zn_{1-x}Co_xTe$ can be attributed to excitations within nearest neighbor Co^{2+} pairs.[13] Although the Co^{2+} concentration ($x=0.01$) in our $Zn_{1-x}Co_xTe$ specimen is smaller than the Mn^{2+} concentration ($x=0.05$) in $Cd_{1-x}Mn_xTe$ for which Peterson *et al.* observed multiple Raman-EPR signatures of Mn^{2+}, it appears that the much stronger *d-d* interaction between Co^{2+} ions in ZnTe ($J_1=38$ K) than that between Mn^{2+} in $Cd_{1-x}Mn_xTe$ (J_1

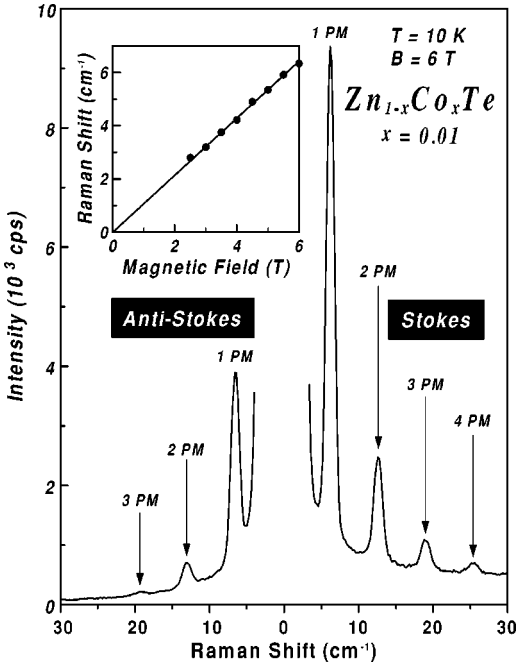

FIG. 5. Stokes (*S*) and anti-Stokes (AS) Raman lines at ω_{PM} generated by spin-flip transitions within the Zeeman multiplet of Co^{2+} in $Zn_{1-x}Co_xTe$ with $x=0.01$. The energy of the exciting laser line $\hbar\omega_L=2.409$ eV; the applied magnetic field $H=6$ T. The external magnetic field **H** (Faraday axis) was applied along the direction of the scattered beam and the incident beam is perpendicular to **H** (Voigt axis) and linearly polarized along **H**.

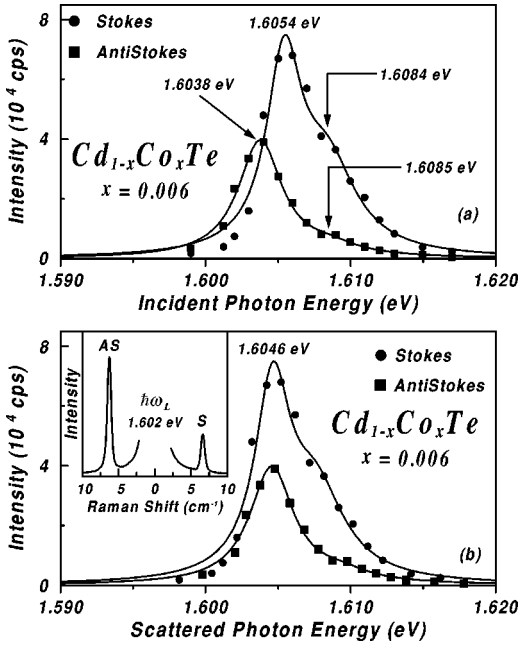

FIG. 6. Resonance profile for the Raman EPR of Co^{2+} in $Cd_{1-x}Co_xTe$ with $x=0.006$ as a function of incident photon energy (a), and scattered photon energy (b). The solid curves are Lorentzian fits to the experimental data. In the inset, a Raman spectrum, excited with $\hbar\omega_L=1.602$ eV, is displayed where an anti-Stokes component is more resonantly enhanced than is the Stokes. The incident beam is along the Voigt axis, and the scattered along the Faraday axis.

$=6.1$ K)[14] allows excitations within nearest-neighbor Co^{2+} pairs in $Zn_{1-x}Co_xTe$ to be observed even with $x=0.01$.

The strong excitonic resonance enhancement in the intensity of the Raman-EPR of Co^{2+} in $Cd_{1-x}Co_xTe$ is displayed in Fig. 6. Raman-EPR intensity as a function of incident photon shows a distinctly different peak for the Stokes as compared to that for the anti-Stokes component as displayed in Fig. 6(a), strongly indicating ''out resonance,'' rather than ''in resonance;'' the ''out-resonance'' character is emphasized in Fig. 6(b), where Raman-EPR intensities for both the Stokes and the anti-Stokes display a maximum at 1.6046 eV *when plotted as a function of scattered photon energy*. The solid lines represent fits with two Lorentzian peaks for the Stokes, as well as for the anti-Stokes components. Besides the main peaks at different incident photon energies in Fig. 6(a), there are shoulders at the *same incident photon energy* (1.6084 eV) for both components, indicating an *in resonance*. The out resonance at 1.6046 eV is associated with the excitonic transition $\Gamma_8:|-3/2\rangle\rightarrow\Gamma_6:|-1/2\rangle$, while that associated with $\Gamma_8:|-1/2\rangle\rightarrow\Gamma_6:|-1/2\rangle$ is responsible for the in-resonance at 1.6084 eV.[15] As a result of this out resonance, the anti-Stokes component is more resonantly enhanced than the Stokes for the exciting energy $\hbar\omega_L<1.603$ eV, as seen in the illustrative example shown in the inset.

C. Raman-EPR and optical phonons in $Cd_{1-x}Co_xTe$ and $Zn_{1-x}Co_xTe$

It is well known that electrons and holes in polar crystals interact strongly with the zone-center LO phonons through the Fröhlich interaction.[16] Being polar semiconductors, $Cd_{1-x}Co_xTe$ and $Zn_{1-x}Co_xTe$ can exhibit the Raman EPR in conjunction with the excitation of LO phonons, appearing with frequency shifts of $\omega_{\mathrm{LO}}\pm\omega_{\mathrm{PM}}$, as first reported by Petrou *et al.*[3] for $Cd_{1-x}Mn_xTe$. The Stokes process with a shift of $\omega_{\mathrm{LO}}+\omega_{\mathrm{PM}}$ involves the creation of an LO phonon and the excitation of a Co^{2+} to the next sublevel of its ground-state Zeeman multiplet, whereas the Stokes shift of $\omega_{\mathrm{LO}}-\omega_{\mathrm{PM}}$ corresponds to the creation of a LO phonon and the deexcitation of a Co^{2+} to the next lower sublevel of the multiplet. The Raman spectrum showing ''CdTe-like'' LO phonon (LO_1) and its EPR satellites is displayed in Fig. 7. The Raman spectrum displaying combinations of LO phonons and EPR signatures obtained in $Zn_{1-x}Co_xTe$ are shown in Fig. 8. Again, the Raman signatures of $LO_1\pm PM$ and $LO_1\pm 2PM$ are distinctly observed. The Co concentration of the specimen ($x\simeq 0.01$) is high enough for the ''CoTe-like'' LO phonon (LO_2) to be observed distinctly. Although the mixed mode behavior of $Zn_{1-x}Co_xTe$ has yet to be systematically investigated, it is reasonable to speculate that it should be similar to that of $Zn_{1-x}Mn_xTe$,[17] the atomic mass of Co (58.9) matching that of Zn (65.4) more closely than does that of Mn (54.9). The very low-solubility limit of Co^{2+} in ZnTe has precluded a comprehensive delineation of the phonon mode behavior of bulk $Zn_{1-x}Co_xTe$. The LO_2+PM is distinctly observed whereas LO_2-PM appears as an unresolved shoulder to the left of the intense LO_1. In the nearly [110] backscattering geometry employed in the experiment, the LO phonons are almost forbidden in all polarization

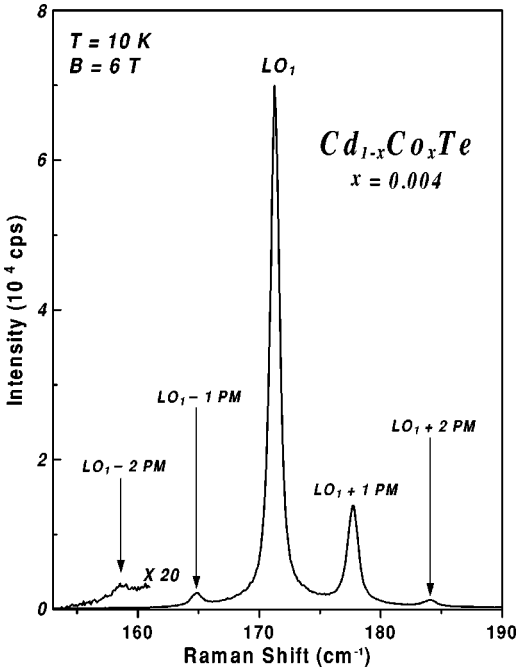

FIG. 7. Raman spectrum displaying ''CdTe-like'' LO phonon (LO_1) and its EPR satellites at frequency shifts $\omega_{LO_1} \pm \omega_{PM}$, $\omega_{LO_1} \pm 2\omega_{PM}$. The sample was excited with $\hbar\omega_L = 1.6215$ eV. The incident beam is along the Voigt axis, and the scattered along the Faraday axis.

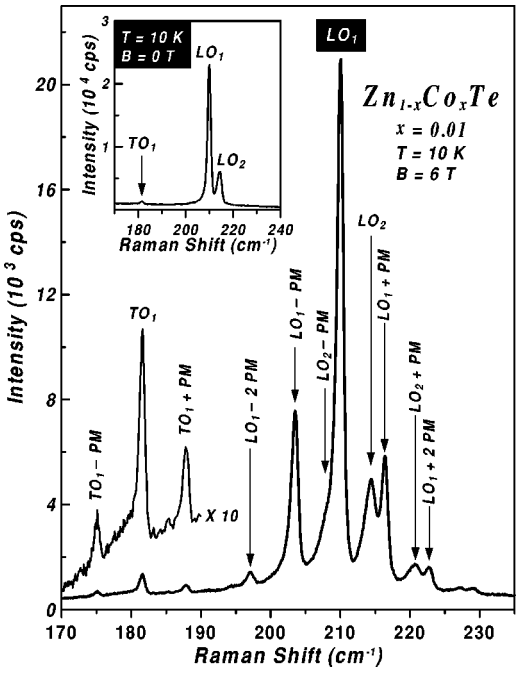

FIG. 8. Raman spectrum displaying ''ZnTe-like'' (LO_1) and ''CoTe-like'' (LO_2) LO phonons together with their EPR satellites at frequency shifts $\omega_{LO} \pm \omega_{PM}$, $\omega_{LO} \pm 2\omega_{PM}$. ZnTe-like TO ($TO_1$) phonon and its EPR satellites are also displayed and enlarged by ten. The inset shows the Raman spectrum without an external magnetic field. The sample was excited with $\hbar\omega_L = 2.409$ eV. The incident beam is along the Voigt axis and the scattered along the Faraday axis. The base lines are shifted vertically for clarity.

configurations.[18] The larger intensity of the LO phonons can be due to a depolarization of the scattered light near resonance induced by Fröhlich interaction, as has been noted by Limmer *et al.*[19]

A striking feature of the Raman spectrum in Fig. 8 is the unmistakable appearance of the ZnTe-like TO (TO_1) mode in combination with the EPR signatures; this is in contrast to the corresponding spectra for $Zn_{1-x}Mn_xTe$ and $Cd_{1-x}Mn_xTe$. We note here that both the Fröhlich interaction and the optical phonon deformation potential can contribute to the electron-phonon interaction in the case of the LO phonon while TO phonons can interact with electrons *only* via the optical phonon deformation potential. In zinc-blende semiconductors, the optical phonon displacement has Γ_4 symmetry and the matrix element of the optical phonon deformation potential between two nondegenerate *s*-like Γ_1 conduction band states is zero, prohibiting deformation-potential interaction between the lowest conduction band electrons and optical phonons in direct band gap semiconductors. In contrast, with the valence band being of Γ_4 symmetry (ignoring spin), the deformation potential interaction with the TO phonon is indeed allowed.[20] Hence, Raman-EPR transitions in combination with TO phonons have to be mediated by the exchange interaction between the valence-band electrons and the *d* electrons of the TMI (*p-d* interaction). The *p-d* exchange interaction in the II-VI DMS's for Co^{2+} is experimentally found to be significantly larger than that for Mn^{2+}.[14] Zielinski *et al.*[21] report a value of (-3030

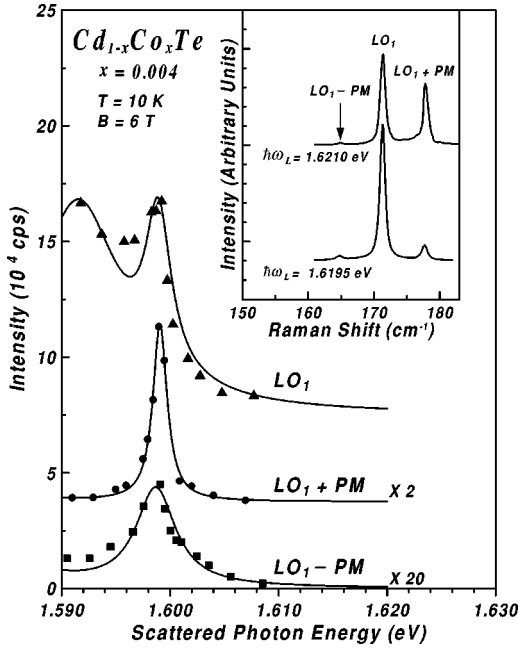

FIG. 9. Resonant Raman profiles for the ''CdTe-like'' LO phonon and its EPR satellites in $Cd_{1-x}Co_xTe$ with $x = 0.004$ as a function of scattered photon energy. The solid curves are Lorentzian fits to the experimental data. The data for $LO_1 + PM$ and $LO_1 - PM$ are enlarged by 2 and 20, respectively. In the inset, Raman spectra, excited with $\hbar\omega_L = 1.6210$ and 1.6195 eV, are displayed as illustrative examples showing out resonance for $LO_1 + PM$ and LO_1, respectively. The incident beam is along the Faraday axis and the scattered along the Voigt axis.

± 150) meV for $N_0\beta$, the *p-d* exchange constant, in $Zn_{1-x}Co_xTe$, which is significantly larger than (-1120 ± 240) meV for Mn^{2+} in $Zn_{1-x}Mn_xTe$, for example.[22] It is also significant that the Co^{2+} *d-d* exchange constant in $Zn_{1-x}Co_xTe$, known to scale with $N_0\beta$,[23] is four times larger than the corresponding constant for Mn^{2+} in $Zn_{1-x}Mn_xTe$. The occurrence of $TO_1 \pm PM$ in $Zn_{1-x}Co_xTe$ and its absence in $Zn_{1-x}Mn_xTe$ can be attributed to the above physical arguments.

The Raman intensities of the ''CdTe-like'' LO phonon and its EPR satellites in $Cd_{1-x}Co_xTe$ exhibits strong resonance enhancement when $\hbar\omega_L$ fulfills the condition for excitonic ''out resonance.'' The Raman intensities, as a function of scattered photon energy, are displayed in Fig. 9, where the solid lines are Lorentzian fits to the experimental data. LO_1, LO_1+PM, and LO_1-PM show strong out resonance with the excitonic transition at 1.599 eV, corresponding to the excitonic Zeeman transition from $\Gamma_8:|-3/2\rangle \rightarrow \Gamma_6:|-1/2\rangle$. In the inset, the Raman spectra, excited with $\hbar\omega_L = 1.6210$ and 1.6195 eV, are displayed as illustrative examples showing out resonance for LO_1+PM and LO_1, respectively.

IV. CONCLUDING REMARKS

The results reported in this paper have revealed examples of Raman EPR in DMS's, viz., those due to the spin flip of the Co^{2+} $3d$ electrons in $Zn_{1-x}Co_xTe$ and $Cd_{1-x}Co_xTe$, yielding g factors of 2.295 and 2.310, respectively. The strong excitonic resonance enhancement in the intensity of the Raman EPR of Co^{2+}, achieved by employing a tunable Ti:sapphire laser, emphasizes that the underlying microscopic mechanism is the strong exchange interaction between Co^{2+} and band electrons in the DMS's. The role of the Fröhlich interaction is brought out in the appearance of the Raman lines at $\omega_{LO} \pm \omega_{PM}$. The large *sp-d* exchange interaction characteristic of the DMS's emerges in a striking manner in the resonance enhancement of $\omega_{LO} \pm \omega_{PM}$. It is anticipated that sufficiently large crystals of $Zn_{1-x}Co_xTe$ and $Cd_{1-x}Co_xTe$ will become available in the near future. This will enable right-angle Raman scattering experiments with well-oriented specimens, allowing a full exploration of the selection rules governing the Raman-EPR transition of Co^{2+} with its T_d site symmetry. In addition, with concentration of Co^{2+} significantly larger than that available to date, it would be of great interest to investigate antiferromagnetic interaction between Co^{2+} ions as manifested in magnon excitations observed in Raman scattering.[9,24] With the introduction of donors, e.g., Cl or In, in these DMS's, the discovery and characterization of the spin-flip Raman scattering from electrons bound to donors would be yet another important problem worthy of study.

ACKNOWLEDGMENTS

The authors acknowledge support from the National Science Foundation Grant No. DMR 98-00858 and Grant No. 94-00415 (Materials Research Science and Engineering Center). The crystals investigated in the present study were grown in the Crystal Growth Facility with support from Purdue University under Academic Reinvestment Program.

[1] *Diluted Magnetic Semiconductors*, edited by J. K. Furdyna and J. Kossut, Semiconductors and Semimetals, Vol. 25 (Academic Press, New York, 1988).

[2] J. A. Gaj, J. Ginter, and R. R. Galazka, Phys. Status Solidi B **89**, 655 (1978).

[3] A. Petrou, D. L. Peterson, S. Venugopalan, R. R. Galazka, A. K. Ramdas, and S. Rodriguez, Phys. Rev. Lett. **48**, 1036 (1982).

[4] A. K. Ramdas and S. Rodriguez, in *Light Scattering in Solids VI*, edited by M. Cardona and G. Güntherodt (Springer-Verlag, Berlin, 1991), pp. 137–206.

[5] D. U. Bartholomew, E-K. Suh, A. K. Ramdas, S. Rodriguez, U. Debska, and J. K. Furdyna [Phys. Rev. B **39**, 5865 (1989)] have studied the Raman-EPR of Co^{2+} in the *wurtzite* $Cd_{1-x}Co_xSe$ for which Co solubility is much higher ($x \geqslant 0.082$) than those for $Zn_{1-x}Co_xTe$ and $Cd_{1-x}Co_xTe$.

[6] I. Miotkowski, H. Alawadhi, M. J. Seong, A. Lewicki, V. Souw, M. McElfresh, A. K. Ramdas, S. Miotkowska, and E. Dynowska, Semicond. Sci. Technol. **16**, 118 (2001).

[7] M. Villeret, S. Rodriguez, and E. Kartheuser, Phys. Rev. B **41**, 10 028 (1990); **42**, 11 375(E) (1990).

[8] J. M. Baranowski, J. W. Allen, and G. L. Pearson, Phys. Rev. **160**, 627 (1967).

[9] A. Petrou, D. L. Peterson, S. Venugopalan, R. R. Galazka, A. K. Ramdas, and S. Rodriguez, Phys. Rev. B **27**, 3471 (1983).

[10] F. S. Ham, G. W. Ludwig, G. D. Watkins, and H. H. Woodbury, Phys. Rev. Lett. **5**, 468 (1960).

[11] D. L. Peterson, D. U. Bartholomew, A. K. Ramdas, and S. Rodriguez, Phys. Rev. B **31**, 7932 (1985).

[12] J. Stühler, G. Schaack, M. Dahl, A. Waag, G. Landwehr, K. V. Kavokin, and I. A. Merkulov, Phys. Rev. Lett. **74**, 2567 (1995).

[13] It should be pointed out that the strength of the overtones are not fully understood quantitatively although this mechanism provides a qualitative account for the observation of multiple Raman-EPR signatures.

[14] D. Heiman, in *High Magnetic Fields in the Physics of Semiconductors II*, edited by G. Landwehr and W. Ossau (World Scientific, Singapore, 1997), pp. 847–856.

[15] H. Alawadhi, Ph.D. thesis, Purdue University, 1999. The six excitonic Zeeman components for the same sample have been measured using wavelength modulated reflectivity (WMR). The excitonic energy gap obtained from the resonant Raman scattering of ''CdTe-like'' LO phonon at zero magnetic field is 4 meV higher than that obtained from WMR. Similar excitonic energy gap differences between resonant Raman scattering and WMR were observed for other specimens with different Co concentrations. A physical explanation for this difference is not yet clear and needs to be explored.

[16] R. Loudon, Proc. R. Soc. London, Ser. A **275**, 218 (1963). For a review, see M. Cardona, *Light Scattering in Solids II*, edited by M. Cardona and G. Güntherodt (Springer, Berlin, 1982), pp. 19–178.

[17] D. L. Peterson, A. Petrou, W. Giriat, A. K. Ramdas, and S. Rodriguez, Phys. Rev. B **33**, 1160 (1986).
[18] See for example, W. Richter, in Springer Tracts in Modern Physics, edited by G. Höhler (Springer, Berlin, 1976), Vol. 78, Table 5.2, p. 176.
[19] W. Limmer, S. Bauer, H. Leiderer, W. Gebhardt, A. Cantarero, C. Trallero-Giner, and M. Cardona, Phys. Rev. B **45**, 11 709 (1992).
[20] P. Y. Yu and M. Cardona, *Fundamentals of Semiconductors* (Springer, Berlin, 1996), pp. 123–127.
[21] M. Zielinski, C. Rigaux, A. Lemaître, A. Mycielski, and J. Deportes, Phys. Rev. B **53**, 674 (1996).
[22] A. Twardowski, Phys. Lett. **94A**, 103 (1983).
[23] B. E. Larson, K. C. Hass, H. Ehrenreich, and A. E. Carlsson, Solid State Commun. **56**, 347 (1985).
[24] S. Venugopalan, A. Petrou, R. R. Galazka, and A. K. Ramdas, Solid State Commun. **38**, 365 (1981).